2018

Effects of Urban Imperviousness Scenarios on Simulated Storm Flow

Feng Pen

Woonsup Choi

Jinmu Choi

Title: Effects of Urban Imperviousness Scenarios on Simulated Storm Flow

Author 1: Feng PAN (fengpan@uwm.edu)

Department of Geography, University of Wisconsin-Milwaukee, P.O. Box 413, Milwaukee, WI 53201-0413, USA

Author 2: Woonsup CHOI, Ph.D. (choiw@uwm.edu)

Department of Geography, University of Wisconsin-Milwaukee, P.O. Box 413, Milwaukee, WI 53201-0413, USA

Author 3 and corresponding author: Jinmu CHOI, Ph.D. (cjm89@khu.ac.kr)

Department of Geography, Kyung Hee University, 26 Kyungheedae-ro, Dongdaemun-gu, Seoul, 02447, Republic of Korea

This is an Accepted Manuscript of an article published by Springer in Environmental Monitoring and Assessment in volume 190 in 2018, available online: https://link.springer.com/article/10.1007/s10661-018-6874-1

Abstract

The amount and distribution of impervious surfaces are important input parameters of hydrological models, especially in highly urbanized basins. This study tests three different methods to input impervious surface area information to a semi-distributed hydrological model in order to examine their effects on storm flow. The three methods being evaluated include: (1) a constant value for impervious surfaces in the entire urban area, (2) constant values of imperviousness for commercial and residential land uses, respectively, and (3) different imperviousness for the residential land use in each subbasin. Storm flow of the Milwaukee River Basin in southeastern Wisconsin (USA) was modeled using the Hydrological Simulation Program–Fortran. The results show that the three methods resulted in substantially different amounts of storm flow. The storm flow simulated with the third method was the largest and had the largest variability among the subbasins. The differences among the scenarios are generally larger in subbasins with high percentage of urban land use types. The results suggest that the effect of different input methods is amplified in urbanized subbasins and the spatial variability of imperviousness should be commensurate with the spatial variability of the model configuration.

Keywords: hydrological model, impervious surface, urban land use, runoff, storm flow

Introduction

Impervious surfaces prevent infiltration of water into the soil, and are used as a measurable indicator of the impacts of urban development on stream ecosystem (Allan 2004). Urban growth inevitably accompanies an increase in impervious surfaces such as rooftops and pavements (Randhir 2003). The increasing extent of impervious surface changes the landscape from an infiltrative sink to a source of runoff (Booth and Jackson 1997). The increasing imperviousness also alters the hydrological cycle by blocking infiltration, increasing runoff production, and reducing lag time between precipitation and runoff peaks, as summarized by Shuster et al. (2005). Such impacts on hydrological processes can be studied using hydrological models where imperviousness is one of input parameters (e.g. Choi and Deal 2008; Caldwell et al. 2012; Dams et al. 2013; Zhou et al. 2014; Sunde et al. 2016; Chen et al. 2017). The amount and distribution of impervious surfaces are important input parameters of hydrological models, especially in highly urbanized basins. Therefore, the way imperviousness data is treated in hydrological models can change the model simulation results.

Imperviousness of land surface is defined by its total extent and the degree to which it is directly connected to the stream channel. The total impervious surface area is the most general measurement of imperviousness, and it is usually expressed as a proportion or percentage of total area (Shuster et al. 2005). Therefore, impervious surface area is a continuous measurement, ranging from 0 to 1 across any land parcel or pixel (Xian et al. 2011). The total impervious surface area in the conterminous United States was found to have increased on average by 4.11%

between 2001 and 2006 (Xian et al. 2011). Moreover, grid cells in the data with high imperviousness increased more than those with low imperviousness (Xian et al. 2011).

Continuous impervious surface percentage can be most accurately derived by utilizing remote sensing data. It can be accomplished by several different methods such as spectral mixture analysis (Wu and Murray 2003; Wu 2004; Lu and Weng 2006), regression tree modeling (Yang et al. 2003a, b; Xian and Crane 2005), decision tree classification (Dougherty et al. 2004), subpixel classification (Civco et al., 2002), neural network classification (Civco and Hurd, 1997), and regression (Bauer et al. 2004, 2005). However, such procedure is not always feasible, e.g. due to data unavailability, or some hydrological models simply cannot use the continuous impervious cover information as input parameters. Instead, such hydrological models require impervious surface information in a discrete manner on a land use/cover class basis, for example, a specific land use/cover class is assigned a specific impervious surface area. Therefore, some input methods are needed to enter continuous imperviousness data in a discrete manner into the hydrological model. Such methods and and their effects on hydrological modeling have been compared by Chormanski et al. (2008), Batelaan et al. (2007), and Voorde et al. (2006). Chormanski et al. (2008) found substantial difference in hydrological modeling results from different impervious surface area input methods. Batelaan et al. (2007) argue that the most accurate imperviousness input should be used for fully-distributed grid-based hydrological models for urban runoff simulation. Voorde et al. (2006) obtained similar results among different input methods for runoff.

The studies by Chormanski et al. (2008), Batelaan et al. (2007), and Voorde et al. (2006) were conducted using grid-based distributed hydrological models. Although distributed hydrologic models can use spatially continuous impervious surface cover as input, they have some disadvantages. Such distributed and physically based models actually are lumped conceptual models with excessive number of parameters, and it can cause very iterative works for both the computer and the researcher during the calibration phase (Beven 1989, 1996). Compared to distributed hydrologic models, semi-distributed hydrological models where the domain is divided into subbasins have less parameters and require less computing capability, thus are more convenient to use. Instead, such models cannot take full advantage of the most accurate impervious surface cover measurements, thus take the imperviousness information in a simplified form.

Our goal in this study was to investigate the extent to which the model results differ between the methods assigning imperviousness. Specifically, we compared the effects of three different imperviousness input methods on storm flow simulated by a semi-distributed hydrological model by modifying the approach adopted by Chormanski et al. (2008). The simulation was conducted for a river basin that has subbasins with varying degrees of urbanization and simple topography. In addition, we examined the results among subbasins with respect to the extent of urban areas in the subbasin.

Study Area

We selected the Milwaukee River basin (US Geological Survey Hydrologic Unit 04040003) located in southeastern Wisconsin as the study area (Figure 1a). It is located between 42° 50′ N and 43° 50′ N latitude, and between 87° 50′ W and 88° 30′ W longitude. The total population of the basin is about 1.3 million, and the basin area is approximately 2267 km^2. The southeast part, where the city of Milwaukee is located, is the most densely populated and urbanized area in the state and contains 90 percent of the population in the basin. The total length of the reaches is about 800 km including the Milwaukee River, Cedar Creek, Menomonee River, and Kinnickinnic River (WDNR 2001). Because the southern portion of the basin is highly urbanized (Figure 1b), storm flow is of great concern in the context of flooding and water quality. When the city of Milwaukee and its suburbs suffered flash flooding in July 2010, even an Individual Assistance Declaration was issued by the President of the United States (FEMA 2010).

Hydrological Model

We selected the Hydrologic Simulation Program-Fortran (HSPF) model (Duda et al. 2012) to simulate storm flow in this study. HSPF is a comprehensive, physically based, semi-distributed hydrological model (Bicknell et al. 1997). Specifically, we used WinHSPF, which is the Windows® interface of HSPF and available as part of the U.S. Environmental Protection Agency's Better Assessment Science Integrating point & Non-point Sources Version 4.1 (U.S. EPA 2013). HSPF has been employed for studying hydrological variables such as streamflow, sediment yield, and non-point source pollution in many projects conducted around the world (e.g. Choi et al. 2017; Alarcon et al. 2009; Hsu et al. 2010; Hayashi et al. 2008; Tzoraki and Nikolaidis 2007).

In HSPF, the study area is divided into subbasins according to topography, and each subbasin contains pervious and impervious land segments and a stream channel (and/or a reservoir). Accordingly, there are three compartments in HSPF to simulate different physical conditions, namely PERLND, IMPLND, and RCHRES. PERLND simulates hydrological processes on pervious land segments, whereas IMPLND is for those on impervious land segments. Both PERLND and IMPLND simulation results will merge into RCHRES and then RCHRES simulates hydraulic processes in a channel or a reservoir. In this study, 33 subbasins were delineated (Figure 1c).

Data

Land use

The land use/land cover data for the Milwaukee River basin (Figure 1b) was obtained from the US Geological Survey (USGS) National Land Cover Database 2001 version, which were derived from satellite imageries from the Multi Resolution Land Characteristics Consortium (Vogelmann et al. 2001). Predominant land use types include planted/cultivated, residential, forest, and wetlands (Table 1).

Table 1. Land use statistics of the Milwaukee River basin

Land use type	Area (km^2)	Percentage (%)
Water	21.2	1.0
Residential	314.0	14.1
Commercial	18.2	1.0
Other urban	382.1	17.2
Forest	240.5	10.8
Shrubland	15.0	0.7
Herbaceous	15.9	0.7
Planted/Cultivated	949.6	42.8
Wetlands	261.7	11.8
Total	**2220.0**	**100**

Imperviousness input for HSPF

We adopted an impervious surface cover percentage dataset (Figure 1c) produced by Li et al. (2018). It was produced by building a linear regression model to predict impervious surface distributions in residential and commercial land uses. The map is a continuous raster data and each grid pixel (30m × 30m) contains a value of impervious surface cover percentage. In order to use it for HSPF, the imperviousness raster data were firstly disaggregated into 33 subbasins and then the average impervious percentages of residential land use types were calculated for each subbasin. Also, the entire raster impervious data and land use map were used together to calculate the average impervious percentage of the commercial land use type. These impervious percentages were then inputted into HSPF during the model setup.

Climate data

The temperature and precipitation input data for HSPF were obtained from the high-resolution gridded daily data sets for Wisconsin (Serbin and Kucharik 2009). The data were produced by interpolating weather stations data across the state to a grid mesh of 8 km by 8 km (Figure 1a) for the period 1950-2006. The gridded data were aggregated to four locations corresponding to the four USGS streamflow gauge stations for the convenience of data input. The four gauge stations are 04086600 Milwaukee River near Cedarburg, 04087000 Milwaukee River at Milwaukee, 04087120 Menomonee River at Wauwatosa, and 04087159 Kinnickinnic River @ S. 11th Street @ Milwaukee (for detailed information regarding the stations, search on http://waterdata.usgs.gov). The Thiessen polygon method (Thiessen 1911) was used to determine the control area for each gauge station. Other weather data were downloaded from the BASINS 4.1 Web site as part of the model package.

Methods

Chormanski et al. (2008) compared three different methods for estimating impervious surface cover on the prediction of peak discharges. The three methods are (1) average percentage of imperviousness for the entire urban area; (2) average percentage of imperviousness for different types of urban land use; and (3) local percentage of imperviousness for every individual cell within the urban area. By using the impervious surface cover percentage map (Figure 1c) and modifying the approach by Chormanski et al. (2008), we developed three scenarios of imperviousness input methods as follows:

Scenario 1 (S1): A constant value for impervious surfaces in the entire urban area

This scenario assumes that the entire urban area has the same impervious surface cover percentage. A spatial mean (29.3%) of the impervious percentage was calculated from the impervious surface cover map (Figure 1c) and was assigned to the entire urban land use for HSPF. Other land use types were assigned zero for impervious percentage value.

Scenario 2 (S2): Constant values of imperviousness for commercial and residential land uses, respectively

In this scenario, commercial and residential land uses were assigned different values of imperviousness. Similar to S1, spatial means of the impervious percentage were calculated but separately for commercial and residential land uses. The commercial land use was assigned a value of 62.2% and the residential land use was assigned a value of 27.3%.

Scenario 3 (S3): Different imperviousness for residential land use of each subbasin

In this scenario, spatial variations of imperviousness of residential land use type were taken into account by assigning a different value of residential imperviousness to each subbasin. As shown in Table 2, the residential land use types of all subbasins were assigned different imperviousness percentage values. The impervious percentage values range from 3.9 % to 94.5 %.

Imperviousness with the highest values is located in highly urbanized subbasins and lowest values located in the rural area. The imperviousness for commercial land uses was fixed at 62.2% in this analysis because their areal extent was very small and their imperviousness did not vary widely by location.

Table 2. Imperviousness percentage of each urban land use type in S3. The numbers in front of 'residential' indicate the subbasin, e.g. '1 residential' means that the residential land in subbasin 1 has an average imperviousness of 7.5%.

Legend	Imperviousness (%)	Legend	Imperviousness (%)
commercial	62.2	17 residential	12.0
1 residential	7.5	18 residential	9.1
2 residential	4.0	19 residential	6.8
3 residential	11.3	20 residential	19.7
4 residential	4.8	21 residential	46.7
5 residential	4.7	22 residential	23.6
6 residential	4.3	23 residential	28.2
7 residential	8.5	24 residential	47.1
8 residential	13.2	25 residential	39.2
9 residential	4.7	26 residential	42.5
10 residential	13.2	27 residential	52.6
11 residential	4.0	28 residential	90.2
12 residential	3.9	29 residential	93.6
13 residential	4.1	30 residential	94.5
14 residential	19.6	31 residential	52.1
15 residential	8.3	32 residential	51.1
16 residential	16.3	33 residential	47.0

The HSPF model was set up using three different scenarios of imperviousness input for the period from January 1986 to December 1995. It was assumed that imperviousness did not change during the time. The time period coincides with that in the study by Choi et al. (2017) where HSPF was applied for the same basin and calibrated. In this study, the three scenarios resulted in total flow values which were different from the observed total flow at Subbasin 21 by less than 4%. The simulated storm flows from the three scenarios were compared graphically and a *t*-test was used to determine if there were significant differences between them. After comparing the simulated storm flow from the three scenarios, the relationships between these differences and the percentage of urban land use across subbasins were examined.

Results and Discussion

Impervious areas from the different imperviousness input methods

Percent imperviousness among the 33 subbasin showed the largest variability with S3 and the smallest variability with S1 (Figure 2). At the same time, the median was largest with S1 and smallest with S3. In S1, 29.3% imperviousness was assigned to all residential and commercial land uses, and a highly urbanized subbasin had imperviousness exceeding 50% whereas as a very rural subbasin had imperviousness of almost 0%. In S3, some subbasins had imperviousness exceeding 60%. Even though residential lands in some subbasins were assigned imperviousness of more than 90%, the subbasins-wide imperviousness remained below 70%. The increasing variability from S1 to S3 is expected since S2 and S3 have more spatial variability of imperviousness values for residential and commercial than S1 and S2, respectively.

Simulated storm flows from the three imperviousness input methods

When averaged across subbasins, S3 resulted in the largest mean annual storm flow with 73.09 mm, followed by S1 (72.63 mm) and S2 (72.47 mm). Because higher imperviousness tends to result in higher storm flow, it is not surprising that S3 resulted in larger mean annual storm flow than S1 and S2. However, the percent differences were small. Storm flow from S3 was larger than S1 by 0.6% and larger than S2 by 0.9%. When it comes to variability among subbasins, S3 resulted in the largest variability and S1 resulted in the smallest (Figure 3). S1 and S2 had very similar variability whereas S3 had a smaller median than S1 and S2, like in Figure 2. Because storm flow is highly influenced by imperviousness in HSPF, the variability of imperviousness among subbasins is reflected on the variability of storm flow among subbasins.

A paired samples *t*-test (n = 33) was conducted between each pair of the three scenarios results. The result illustrates that all three pairs of scenarios are significantly different (Table 3). S1 and S2 produced very similar annual storm flows (Figure 3), but their difference is found to be nonetheless significant. As mentioned above, the differences were no larger than 1%. Even larger percent differences could result from model configuration and other factors. Therefore, the effect of the imperviousness input methods is deemed negligible when the results are averaged across subbasins.

Table 3. Paired samples *t*-test for annual storm flows (mm) of three scenarios

Pair	Paired errors Mean	St. dev.	Standard Error	95% confidence interval Lower	Upper	Sig. (2-tails)
S1-S2	4.32E-04	2.17E-03	3.59E-05	3.61E-04	5.02E-04	0.00
S1-S3	-1.69E-03	2.10E-02	3.48E-04	-2.38E-03	-1.01E-03	0.00
S2-S3	-1.26E-03	2.15E-02	3.56E-04	-1.96E-03	-5.64E-04	0.00

The relationship between simulated storm flow differences and percentage of urban land use

Figure 4 portrays the spatial distribution of the differences of simulated storm flow between any two scenarios. Like in Figure 3, the difference between S1 and S2 (Figure 4a) is not as large as the difference involving S3 (Figures 4b and 4c) across the subbasins. Between S1 and S2, largest differences were found in subbasins 25, 26, and 27 and the magnitude is up to 24 mm. Figures 4b and 4c show clusters of large differences in the downstream subbasins and the difference is larger than 60 mm in some subbasins. As seen in Figures 1b and 1c, they are heavily urbanized and impervious subbasins. On the other hand, upstream subbasins show very small differences in storm flow regardless of the scenario pairs. Therefore, the effect of different input methods appears to be amplified in urbanized subbasins.

The simulated storm flow differences and the urbanized land use percentage were positively correlated ($p < 0.05$) for all pairs (Figure 5). For the S1-S2 pair (Figure 5a), the urban percentage explains only 16% of the variability of storm flow differences and the correlation is weak. For the other two pairs, r^2 values are much higher and the slopes are steeper (> 0.4). Overall, in more urbanized subbasins, the effects of imperviousness input methods tend to be larger. In other words, the way imperviousness information is handled in a hydrological model matters much more in urbanized areas than rural ones.

In Figure 5a, there are two cases (subbasins 21 and 28) that may be considered as outliers. Both subbasins are very small and located in an area of stream intersection (Figure 6). We speculate that subbasins with such small sizes can be very sensitive to the change of imperviousness input. Figures 5b and 5c also show some outliers, well below or above the regression lines. These figures involve S3, where the residential land use type was assigned different imperviousness values whereas the commercial land use was assigned a constant one. Thus, if some subbasins are mostly covered by commercial land use, the differences from different imperviousness input methods would be very small. Subbasins 28 to 30 are such cases. Subbasins 21 and 25 have similar imperviousness across the scenarios, at about 40%. As a result, the differences in storm flow are quite small. For subbasins with high urban percentage values and well above the regression line, such as 24, 26, 27, 31, and 32, imperviousness input increased substantially from S1 or S2 to S3.

This study found significant differences among the results from different imperviousness input methods similar to Chormanski et al. (2008). However, unlike Chormanski et al. (2008), this study used a semi-distributed hydrological model instead of a fully distributed model. The raster-based imperviousness data have been aggregated to different levels of spatial variability to be input to the hydrological model. For a study using a semi-distributed model, this aggregation process was necessary and lead to statistically significantly different results. Aggregation for each subbasin (S3) resulted in particularly different results for urbanized subbasins from aggregations for the entire basin (S1 and S2).

Conclusions

This study tested three different methods to input imperviousness information to a semi-distributed hydrological model to examine their effects on model-simulated storm flow. The three methods evaluated include: (1) a constant value for impervious surfaces in the entire urban area, (2) constant values of imperviousness for commercial and residential land uses, respectively, and (3) different imperviousness for the residential land use in each subbasin. The methods represent increasing spatial variability of imperviousness values in residential land use. Storm flow of the Milwaukee River basin was simulated by HSPF using the three imperviousness input methods.

The study found very small but statistically significant differences in spatially-averaged annual storm flows between the methods. In a qualitative sense, we think the differences are negligible. However, the differences were generally larger in more urbanized subbasins. The results were particularly different when imperviousness values were differently assigned for each subbasin.

Therefore, we conclude that the spatial variability of imperviousness should be commensurate with the spatial variability of the model configuration. Even though impervious surface area data are available as a continuous, high-resolution raster data set, the way it is used for a semi-distributed hydrological model can produce different results. Aggregating the impervious surface are data for the entire basin negates the spatial variability of storm flow simulated by the semi-distributed hydrological model.

Reference

Alarcon VJ, Mcanally W, Diaz-Ramirez J, Martin J, and Cartwright J. (2009) A Hydrological Model of the Mobile River Watershed, Southeastern USA. AIP Conference Proceedings 1148: 641-645

Allan JD (2004) Landscapes and riverscapes: The influence of land use on stream ecosystems. Annu Rev Ecol syst 35:257-284

Batelaan O, Chormanski J, Canters F, and Van de Voorde T (2007) Improved distributed runoff modelling of urbanised catchments by integration of multi-resolution remote sensing. Geoscience and Remote Sensing Symposium. IGARSS 2007. IEEE International. 23-28 July 2007. 5021-5024

Bauer ME, Heinert NJ, Doyle JK, Yuan F (2004) Impervious surface mapping and change monitoring using satellite remote sensing. Proceedings, American Society of Photogrammetry and Remote Sensing Annual Conference. May 24-28, Denver, Colorado. unpaginated CD ROM 10 pp

Bauer M, Loeffelholz B, Wilson B (2005) Estimation, mapping and change analysis of impervious surface area by Landsat remote sensing. Proceedings, Pecora 16 Conference, American Society of Photogrammetry and Remote Sensing. October 23 - 27, 2005, Sioux Falls, South Dakota. unpaginated CD ROM 9 pp

Beven K (1989) Changing ideas in hydrology-The case of physically-based models. Journal of Hydrology 105:157-172

Beven K (1996) A Discussion of Distributed Hydrological Modelling. In: Abbott M, Refsgaard J (eds.) Distributed Hydrological Modelling. Springer Netherlands.

Bicknell BR, Imhoff JC, Kittle JL Jr, Donigian AS Jr, Johanson RC (1997) Hydrological Simulation Program--FORTRAN User's Manual for Version 11: Project Summary, U.S. Environmental Protection Agency, National Exposure Research Laboratory.

Booth DB, Jackson CR (1997) Urbanization of aquatic systems: Degradation thresholds, stormwater detention, and limits of mitigation. J Am Water Resour Assoc 33:1077-1090

Caldwell PV, Sun G, Mcnulty SG, Cohen EC, Moore Myers JA (2012) Impacts of impervious cover, water withdrawals, and climate change on river flows in the conterminous US. Hydrol Earth Syst Sci 16:2839-2857

Chen J, Theller L, Gitau MW, Engel BA, Harbor JM (2017). Urbanization impacts on surface runoff of the contiguous United States. Journal of Environmental Management, 187, 470-481.

Choi W, Deal BM (2008). Assessing hydrological impact of potential land use change through hydrological and land use change modeling for the Kishwaukee River basin (USA). Journal of Environmental Management, 88(4), 1119-1130.

Choi W, Pan F, Wu C (2017). Impacts of climate change and urban growth on the streamflow characteristics of the Milwaukee River (Wisconsin, USA). Regional Environmental Change, 17(3), 889-899. DOI: 10.1007/s10113-016-1083-3

Chormanski J, Van De Voorde T, De Roeck T, Batelaan O, Canters F (2008) Improving Distributed Runoff Prediction in Urbanized Catchments with Remote Sensing based Estimates of Impervious Surface Cover. Sensors 8:910-932

Civco DL, Hurd JD (1997) Impervious surface mapping for the state of Connecticut, Proceedings, American Society for Photogrammetry and Remote Sensing Annual Conference, April 7-10, Seattle, Washington, Missouri, pp.3:124-135.

Civco DL, Hurd JD, Wilson EH, Arnold CL, Prisloe MP Jr (2002) Quantifying and describing landscapes in the northeast United States, Photogrammetric Engineering and Remote Sensing 68(10):1083-1090

Dams J, Dujardin J, Reggers R, Bashir I, Canters F, Batelaan O (2013) Mapping impervious surface change from remote sensing for hydrological modeling. Journal of Hydrology 485:84-95

Dougherty M, Dymond RL, Goetz SJ, Jantz CA, Goulet N (2004) Evaluation of impervious surface estimates in a rapidly urbanizing watershed. Photogrammetric Engineering and Remote Sensing 70(11):1275-1284

Duda PB, Hummel PR, Donigian AS Jr, Imhoff JC (2012) BASINS/HSPF Model Use, Calibration and Validation. Transactions of the ASABE 55(4):1523-1547

Federal Emergency Management Agency (FEMA) (2010) President Declares Individual Assistance for Grant and Milwaukee Counties. http://www.fema.gov/news-release/2010/09/18/president-declares-individual-assistance-grant-and-milwaukee-counties (last accessed 12 November 2016)

Hayashi S, Murakami S, Kai-Qin X, Watanabe M, Bao-Hua X (2008) Daily Runoff Simulation by an Integrated Catchment Model in the Middle and Lower Regions of the Changjiang Basin, China. Journal of Hydrologic Engineering 13:846-862

Hsu SM, Chiou LB, Lin GF, Chao CH, Wen HY, Ku CY (2010) Applications of simulation technique on debris-flow hazard zone delineation: a case study in Hualien County, Taiwan. Nat Hazards Earth Syst Sci 10:535-545

Li, W., Wu, C., Choi, W. (2018). Predicting future urban impervious surface distribution using cellular automata and regression analysis. Earth Science Informatics 11(1): 19-29. DOI: 10.1007/s12145-017-0312-8

Lu D, Weng Q (2006) Use of impervious surface in urban land-use classification, Remote Sensing of Environment 102(1-2):146-160

Randhir T (2003) Watershed-scale effects of urbanization on sediment export: Assessment and policy. Water Resour. Res. 39(6):1169

Serbin SP, Kucharik CJ (2009) Spatiotemporal Mapping of Temperature and Precipitation for the Development of a Multidecadal Climatic Dataset for Wisconsin. Journal of Applied Meteorology and Climatology 48:742-757

Shuster WD, Bonta J, Thurston H, Warnemuende E, Smith DR (2005) Impacts of impervious surface on watershed hydrology: A review. Urban Water Journal 2:263-275

Sunde M, He HS, Hubbart JA, Scroggins C (2016). Forecasting streamflow response to increased imperviousness in an urbanizing Midwestern watershed using a coupled modeling approach. Applied Geography, 72: 14-25.

Thiessen AH (1911) Precipitation for large areas. Monthly Weather Review 39:1082–1084

Tzoraki O, Nikolaidis NP (2007) A generalized framework for modeling the hydrologic and biogeochemical response of a Mediterranean temporary river basin. Journal of Hydrology 346:112-121

U.S. EPA (Environmental Protection Agency) (2013) Watershed modeling to assess the sensitivity of streamflow, nutrient, and sediment loads to potential climate change and urban development in 20 U.S. watersheds. National Center for Environmental Assessment, Washington, DC; EPA/600/R-12/058F. Available from the National Technical Information Service, Alexandria, VA, and online at http://www.epa.gov/ncea.

Vogelmann JE, Howard SM, Yang L, Larson CR, Wylie BK, Driel JNV (2001) Completion of the 1990's National Land Cover Data Set for the conterminous United States. Photogrammetric Engineering and Remote Sensing 67:650-662

Voorde TVD, Chormanski J, Batelaan O, Canters F (2006) Multi-resolution impervious surface mapping for improved runoff estimation at catchment level 1st EARSeL Workshop of the SIG Urban Remote Sensing. Humboldt-Universität zu Berlin, 2-3 March 2006.

Wisconsin Department of Natural Resources (WDNR) (2001) The State of the Milwaukee River basin. Madison, Wisconsin: Wisconsin Department of Natural Resources, PUBL WT 704 2001

Wu C (2004) Normalized spectral mixture analysis for monitoring urban composition using ETM+ imagery, Remote Sensing of Environment 93(4):480-492

Wu C, Murray AT (2003) Estimating impervious surface distribution by spectral mixture analysis. Remote Sensing of Environment 84(4):493-505

Xian G, Crain M (2005) Assessments of urban growth in Tampa Bay watershed using remote sensing data. Remote Sensing of Environment 97(2):203-215

Xian G, Homer C, Dewitz J, Fry J, Hossain N, Wickham J (2011) Change of Impervious Surface Area Between 2001 and 2006 in the Conterminous United States. Photogrammetric Engineering and Remote Sensing 77:758-762.

Yang L, Huang C, Homer CG, Wylie BK, Coan MJ (2003) An approach for mapping largearea impervious surfaces: synergistic use of Landsat-7 ETM+ and high spatial resolution imagery. Canadian Journal of Remote Sensing 29(2):230-240

Yang L, Xian G, Klaver JM, Deal B (2003) Urban land cover-change detection through subpixel imperviousness mapping using remotely sensed data. Photogrammetric Engineering and Remote Sensing 69(9):1003-1010

Zhou Y, Wang Y, Gold A, August P, Boving T (2014) Assessing impact of urban impervious surface on watershed hydrology using distributed object-oriented simulation and spatial regression. GeoJournal 79:155-166

Figure Captions

Fig. 1. Boundaries of the Milwaukee River basin and 33 delineated subbasins. (A) elevation, stream network, and climate data grid; (B) land use distribution; (C) percent imperviousness by pixel

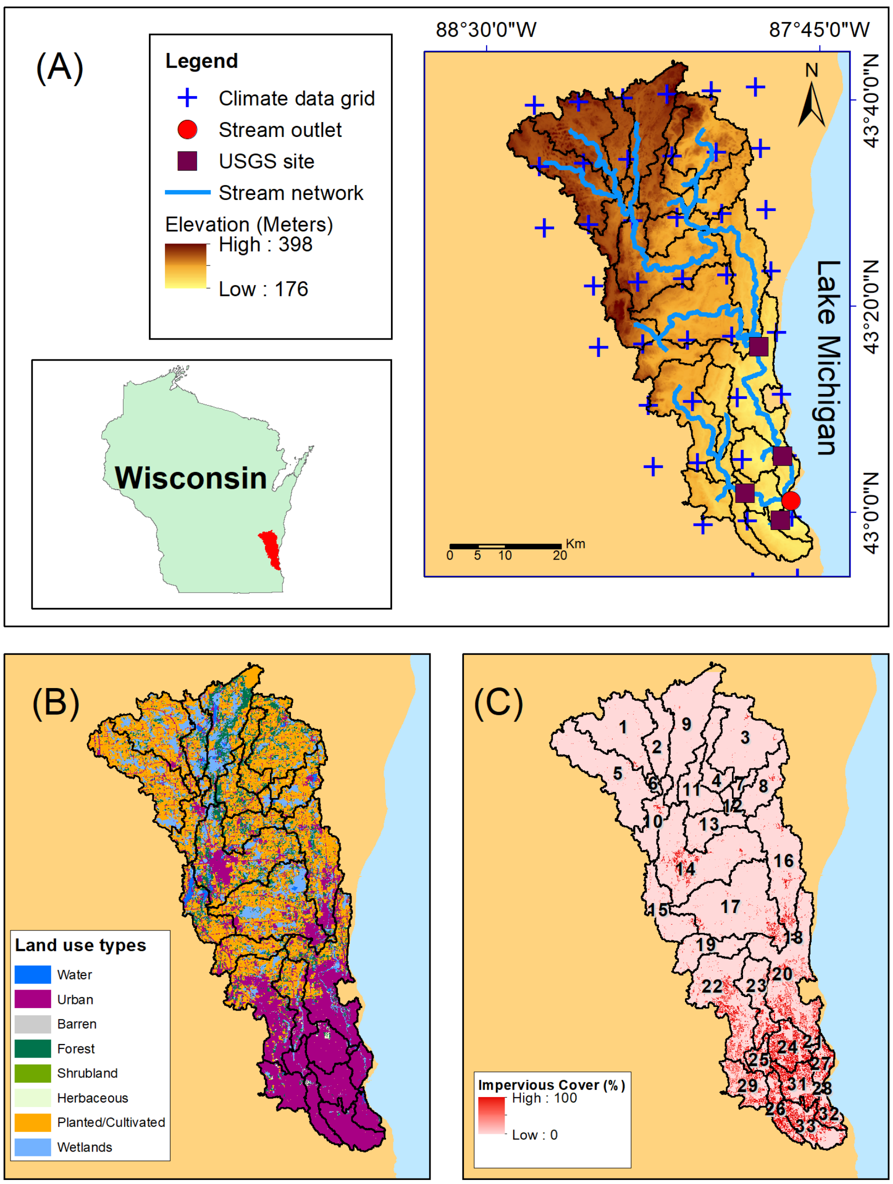

Fig. 2. Boxplots of impervious percentage from the three imperviousness input methods. The variability is among the 33 subbasins

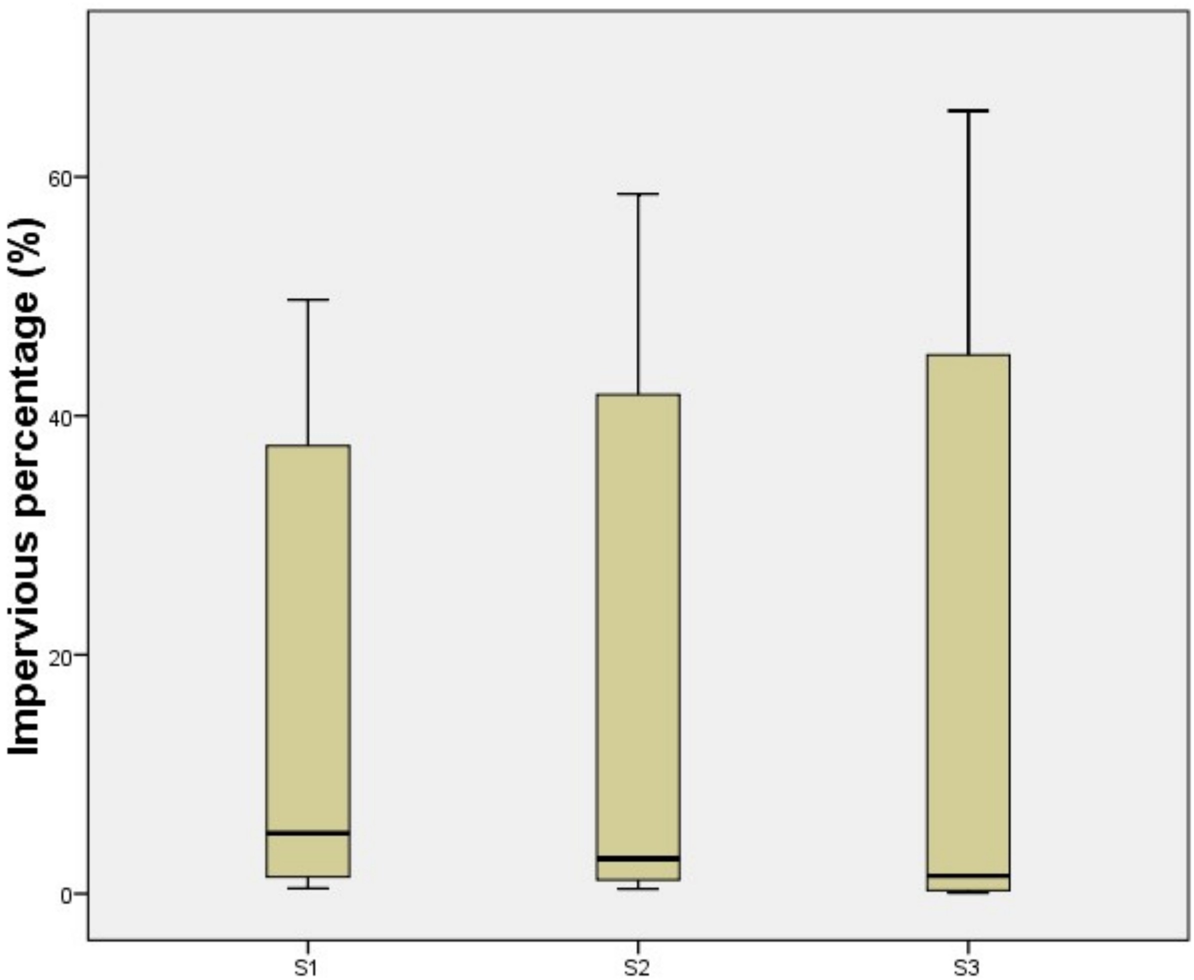

Fig. 3. Boxplots of the simulated storm flow using the three imperviousness input methods for the 33 subbasins

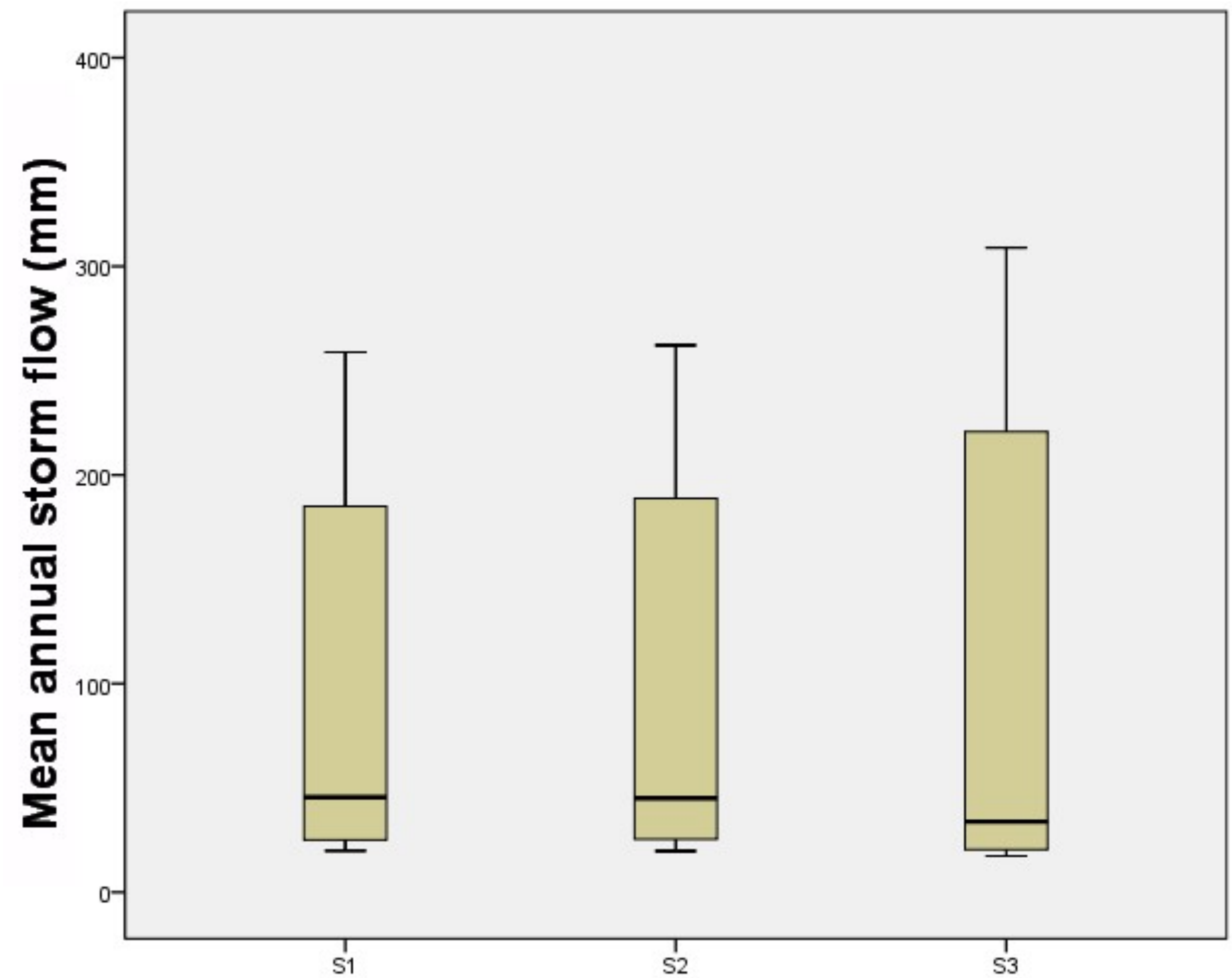

Fig. 4. Storm flow differences by subbasin between S1 and S2 (A), S2 and S3 (B), and S1 and S3 (C) (the differences were calculated as the latter minus the former)

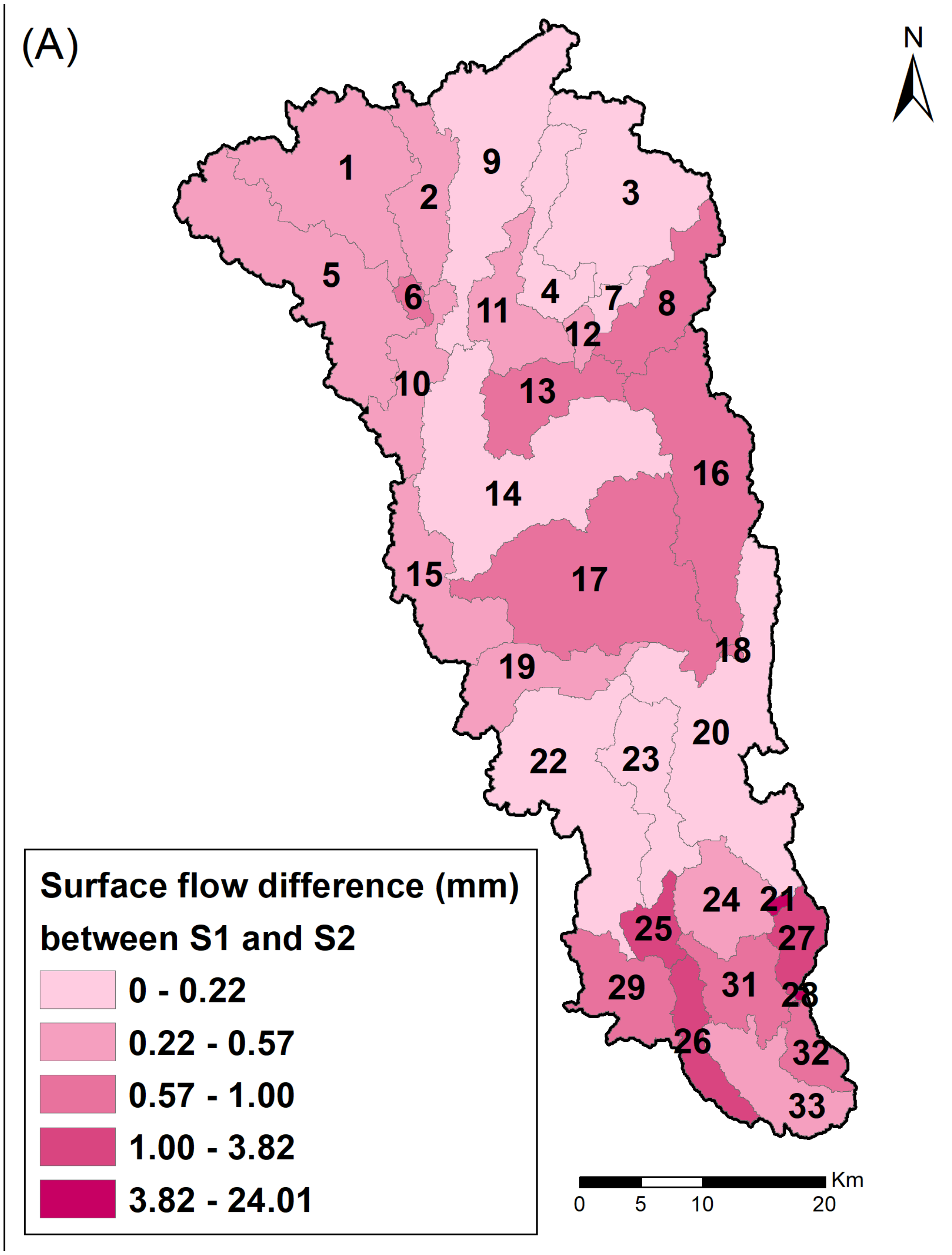

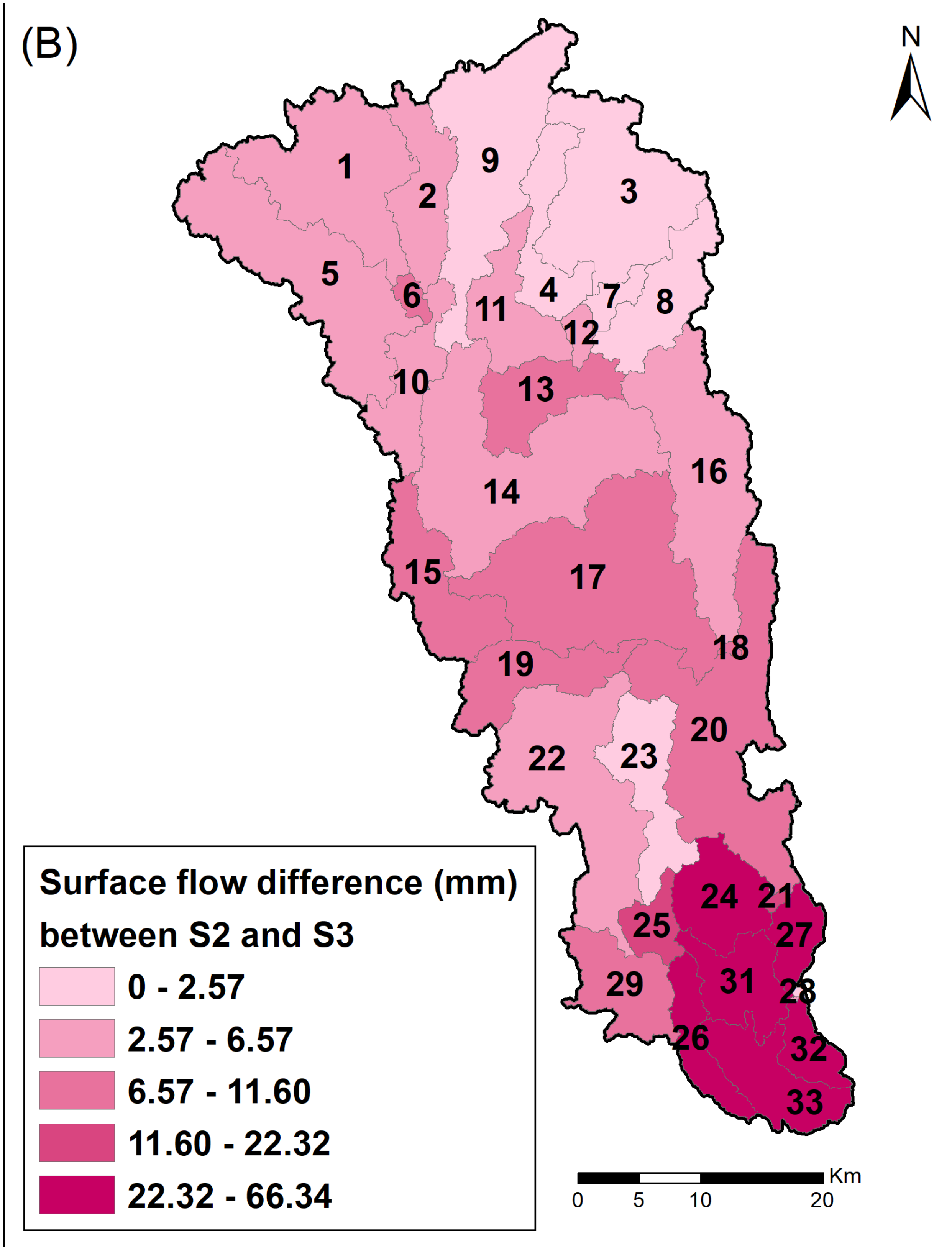
(B)
N
1
2
3
4
5
6
7
8
9
10
11
12
13
14
15
16
17
18
19
20
21
22
23
24
25
26
27
28
29
31
32
33
Surface flow difference (mm) between S2 and S3
0 - 2.57
2.57 - 6.57
6.57 - 11.60
11.60 - 22.32
22.32 - 66.34
Km
0
5
10
20

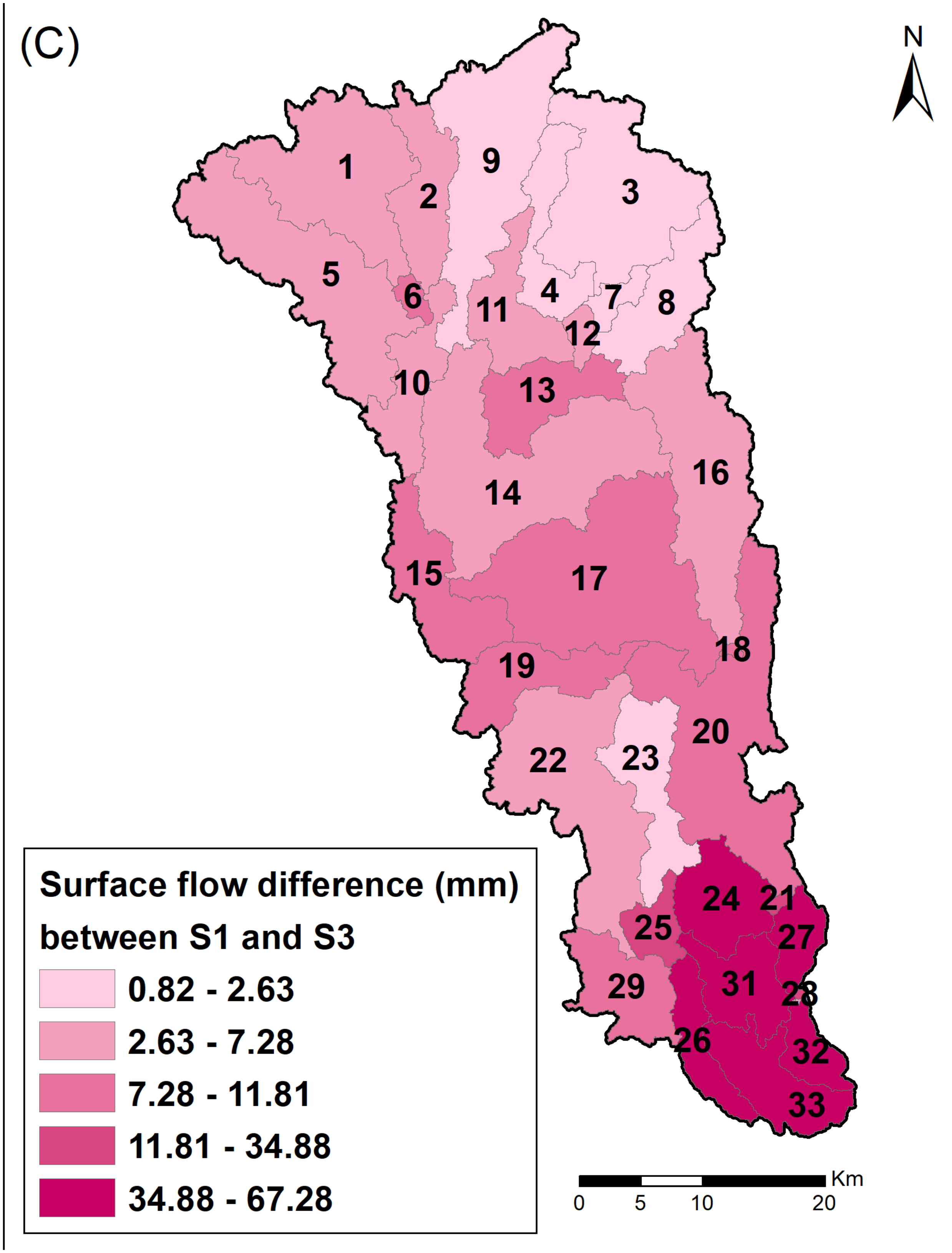
(C)
N
1
2
3
4
5
6
7
8
9
10
11
12
13
14
15
16
17
18
19
20
21
22
23
24
25
26
27
28
29
31
32
33
Surface flow difference (mm)
between S1 and S3
0.82 - 2.63
2.63 - 7.28
7.28 - 11.81
11.81 - 34.88
34.88 - 67.28
Km
0
5
10
20

Fig. 5. Linear regression between the urban percentage and storm flow differences across subbasins

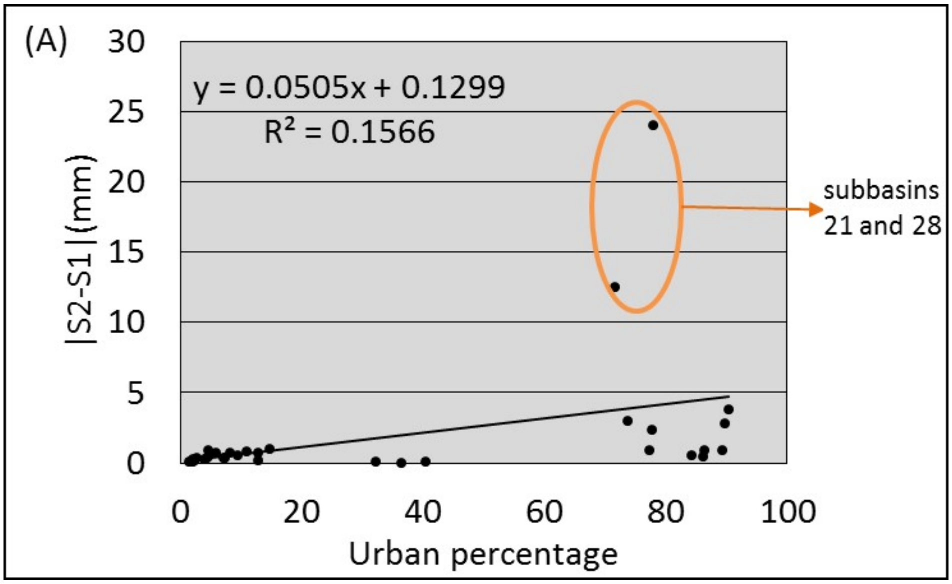

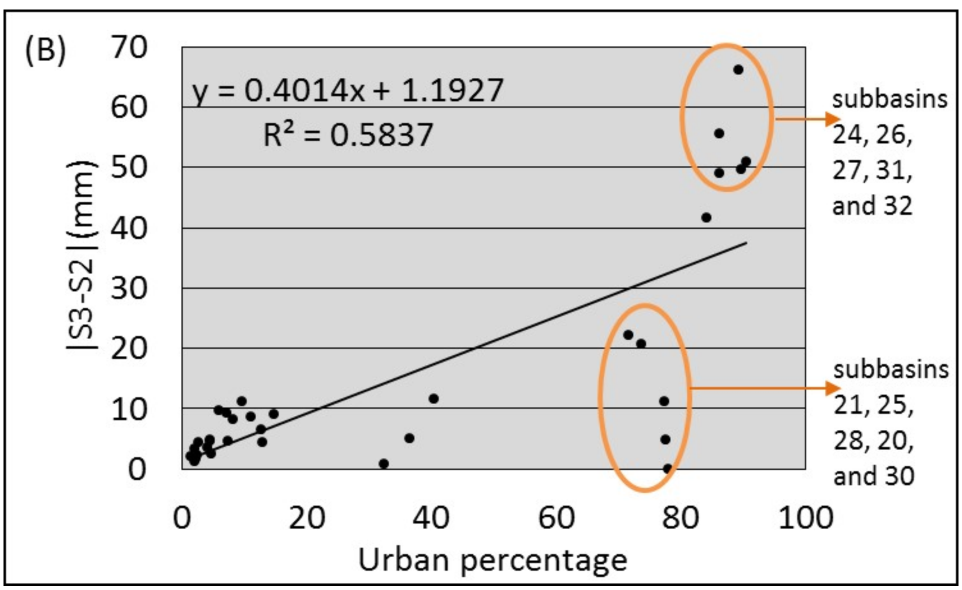

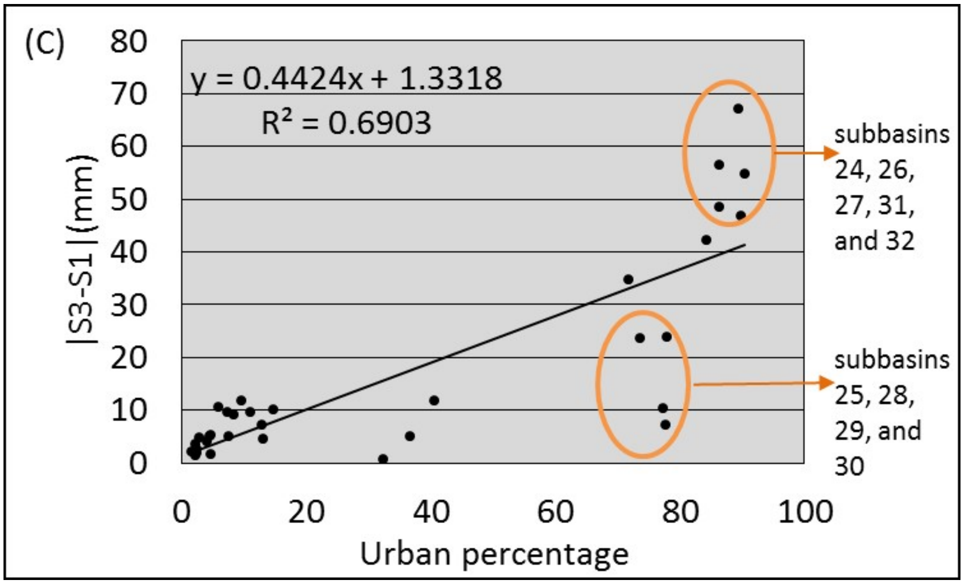
(C)
y = 0.4424x + 1.3318
R² = 0.6903
|S3-S1| (mm)
Urban percentage
0
10
20
30
40
50
60
70
80
0
20
40
60
80
100
subbasins 24, 26, 27, 31, and 32
subbasins 25, 28, 29, and 30

Fig. 6. Residential and commercial grid pixels of downstream subbasins